© 2019 IJSRSET | Volume 6 | Issue 3 | Print ISSN: 2395-1990 | Online ISSN : 2394-4099
Themed Section : Engineering and Technology
DOI : https://doi.org/10.32628/IJSRSET196312

Using Landsat-8 Data in Preliminary Exploration for Geothermal Resources

Kathurima C. Eric

Geothermal Energy Training and Research Institute, Dedan Kimathi University of Technology, Nyeri, 10100, Kenya

eric.kathurima@dkut.ac.ke

ABSTRACT

To characterize geothermal potential areas, conventional surface exploration activities involve field surveys, gathering geothermal information from locals and review of any existing geothermal literature. This is not only time consuming and costly but also unreliable for inaccessible geothermal potential areas. Thus, this study explores the cost-effectiveness and powerful tools of satellite remote sensing in preliminary land surface characterization for expansive geothermal exploration. The main approach entailed the use of free-access Landsat-8 and atmospheric data to retrieve land surface temperature (LST) using split-window and single channel algorithm, analysis of retrieved surface products, validation using in-situ ground temperature data, and finally delineation of surface thermal anomalies associated with geothermal features. Gilgil district and Baringo County in Kenya made the study areas. The former is a known and confirmed geothermal area while the latter is only a geothermal prospect. The two areas sit on the central section of the Kenyan rift; geothermal belt, and combined form a suitable case study for preliminary exploration using Landsat-8 data. The main objective of the study was to demonstrate the use of satellite remote sensing data to identify surface thermal anomalies associated with geothermal features as a cost-effective geothermal exploration support tool. Identify the best LST retrieval method between split window and single channel method using Landsat 8 data, and finally employ the better retrieval method to characterize geothermal prospect area and suggest targets for further investigations. Results showed that free-access satellite remote sensing imagery can conveniently be used to identify and map surface thermal anomalies associated with geothermal features and thus can be employed to complement the main geothermal exploration studies namely geological, geochemical and geophysical. Further, single channel method had better LST retrieval results compared to split-window method when using Landsat-8 data.

Keywords : Land Surface Temperature, Landsat-8, Geothermal, Split Window, Single Channel, Thermal Anomalies

I. INTRODUCTION

Surface geothermal exploration studies under the three main geothermal exploration investigations namely geological, geochemical, and geophysical seeks to characterize explored areas into different potential levels of the underlying geothermal resources, and identification of target areas for detailed investigations through mapping and delineation. This form of preliminary investigations leads to categorization of an area into geothermal potential or non-geothermal. Geothermal potential areas are further divided into three broad categories of high, medium and low enthalpy geothermal areas. To enhance exploration results, new techniques and approaches are being employed to provide among others expanded areal coverage within short periods of time, rapid data collection and analysis, and cost-effective methods aimed at lowering exploration cost. Land surface temperature and thermal anomalies detection and mapping using high and medium spatial resolution satellite remote sensing data is such one approach.

Land surface temperature (LST) is one of the integral parameters in surface energy and water balance processes at all scales; from local to global [1]–[3]. As a result, LST is widely used in many fields including

global and regional climate change studies, heat islands and urban climate, agricultural water monitoring and management, environmental studies, geothermal exploration and vegetation monitoring among others [4]. LST derived from satellite remote sensing data provides extensive area coverage with sufficient spatial and temporal resolution making surface temperature studies and investigations even at global scale quite feasible.

Satellite remote sensing data has been used to aid geothermal exploration efforts through detection and identification of surface thermal anomalies associated with geothermal features and systems. Subsequently, identification of geothermal features of interest for further investigations has been possible. [5] Used spaceborne and airborne imagery to explore for geothermal potential of Barrier Volcanic complex in Kenya by mapping of thermal anomalies, mineralogy, geological features and hot spots. Using satellite thermal infrared remote sensing data, temperature anomalies of surface geothermal attributes including hot springs, geysers, heated ground, and fumaroles have been delineated [6]. Surface thermal anomalies associated with geothermal features over geothermal areas have also been detected [7]–[10]. Advanced Spaceborne Thermal Emission and Reflection Radiometer (ASTER) and Landsat satellite series have been the source of free-access thermal infrared data used in many surface temperature studies [11]–[16].

Landsat 8 satellite is the latest in the Landsat Program series. It was launched in February 2013 to provide data continuity with previous Landsat mission, Landsat 4 – 7, as one of its main objectives. L8 carries two sensor instruments; Operational Land Imager (OLI) and Thermal Infrared Sensor (TIRS). Both sensors are of pushbroom type. The L8 Observatory (the spacecraft with its two integrated sensors) operates in a Sun-synchronous orbit with a 705 km altitude at the Equator, and a 16-day repeat cycle. OLI and TIRS sensors simultaneously image every scene thus providing coincident image of the same surface area with a 185 km swath width. Further, data from the two sensors is radiometrically corrected and co-registered to a cartographic projection to correct for terrain displacement to produce standard orthorectified digital images; Level 1T product data [17].

TIRS collects image data for two thermal bands covering wavelength range 10.0-12.5 μm at 100 m spatial resolution. With two adjacent thermal bands, L8 Observatory presents an advancement over the single-band thermal data of previous Landsat mission (i.e. Landsat 4-7). Further, TIRS spatial resolution of 100 m is lower and coarser than 60 m spatial resolution of its predecessor ETM+ thermal band; band 6. However, the presence of dual thermal bands in TIRS allows the use of split window techniques for atmospheric correction and land surface temperature retrieval although caution ought to be observed due to stray light issues with Band 11 [17]. The ability of L8 Observatory's TIRS instrument to collect data for two narrow spectral and adjacent thermal bands in the thermal region formerly covered by one wide spectral band in Landsat 4-7, has seen an increase in use of techniques such as split window in atmospheric correction and LST retrieval from L8 data [15], [16], [18].

Depending on data availability, any or both single channel and split window method can be applied in land surface temperature retrieval. Different versions of single channel methods or algorithms require only one thermal infrared band to retrieval LST of a region of interest [1], [9], [12], [19]. On the other hand, split window methods (also referred to as two-channel method) require two thermal infrared bands in the atmospheric window of the electromagnetic spectrum (i.e. 10 – 12 μm) to retrieve land surface temperature [1], [2], [20].

In this paper, two LST retrieval methods namely split-window and single channel algorithm are used to retrieve land surface temperature and identification of surface thermal anomalies associated with geothermal resources using Landsat 8 data. The two methods were chosen for the study due to their functional applicability to Landsat 8 data that has two thermal infrared channels in the atmospheric window. Two study areas in Kenya were considered; Gilgil district, a known geothermal area comprising of Eburru-Jika-Badlands-Elementainta geothermal area, and Baringo County, a geothermal prospect area. In the first case, the two retrieval methods were applied to Landsat-8 data of the known geothermal area and their retrieved LST and identified surface thermal

anomalies associated with geothermal features validated using in-situ ground temperature data and observed features. After the validation process, single channel method having superior results compared to split window algorithm when using Landsat-8 data, was employed in the second case to retrieve LST and identify surface thermal anomalies associated with geothermal features and systems in the second study area, a geothermal potential area. Geothermal prospects from analysis of the identified surface thermal anomalies with existing geothermal information of the area were eventually identified and recommended for further investigations

II. METHODS AND MATERIAL

A. Study area

This study was first carried out in a known geothermal field; Gilgil district, and later in a geothermal prospect area; Baringo County. The rationale behind this sequence was to identify the best method for land surface temperature retrieval from Landsat-8 data and the subsequent detection of thermal anomalies associated with geothermal features between single channel and split window methods. Thereafter, the better method was applied on a geothermal prospect area to detect, identify and delineate geothermal anomalous areas. These would then be recommended for detailed investigations using high resolution exploration methods e.g. ground survey or unmanned aerial vehicles (UAVs).

Known geothermal area: Eburru-Badlands-Elemeintaita geothermal areas of Gilgil district, Nakuru County, Kenya.

The dominant surface geothermal features of this study area include fumaroles, warm and steaming grounds, and hydrothermally altered grounds. The area also boost of an active geothermal power plant with a capacity of 2.5 MWe and several exploration wells at Eburru geothermal area. The three highlighted areas within this study area are considered to have sufficient geothermal potential for commercial exploitation based on analysis of geothermal exploration studies [21].

Geothermal prospect area: Baringo County, Kenya.
The notable geothermal prospects areas in this study area include Lake Baringo, Korosi, Chepchuk and Paka. All these prospects are located in the northern part of the Kenya Rift and sits within the central sector of the rift system. Weak fumarolic activities, hot springs, thermally altered grounds, and steaming grounds are the notable surface geothermal manifestations [22].

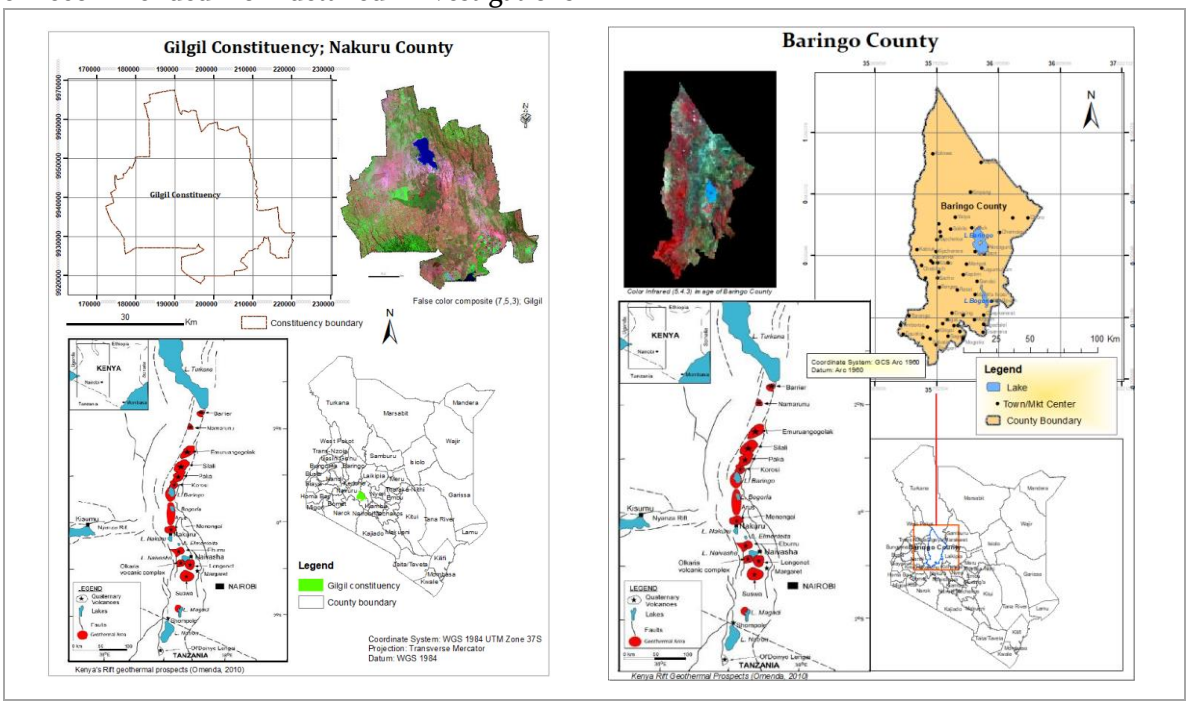

Fig. 1 Study areas: Known geothermal area (left) and geothermal prospect area (right). Kenya's geothermal prospects map [22]

B. Data

The data used in the study was obtained from different sources. Table 1 below enumerates the data used and summarizes key information and characteristics.

Table 1. Data and sources

Data	Data Type	Spatial Reference	Data Source	Description
Landsat 8	Raster	WGS-84, UTM	U.S. Geological Survey (USGS)	OLI and TIRS data
Water vapor content	Numeric	MODIS sinusoidal projections	LP DAAC located at USGS/EROS	MODIS MOD05_L2
Administrative boundaries	Vector	Universal Transverse Mercator (UTM)	Independent Electoral and Boundaries Commission (IEBC, Kenya)	Boundaries shapefiles
Demographic & settlement	Vector	UTM	Kenya National Bureau of Statistics (KNBS)	Towns and market centers (Baringo County)

Landsat 8 Operational Land Imager (OLI) and Thermal Infrared Sensor (TIRS) data and MODIS MOD05_L2 water vapor product were the two main data types in the study. Landsat 8 data was retrieved from the U.S. Geological Survey through https://earthexplorer.usgs.gov while MODIS water vapor data from NASA (National Aeronautics and Space Administration) Land Processes Distributed Active Archive Center (LP DAAC) products was downloaded from http://lpdaac.usgs.gov. The rest of the data types were sourced from government agencies and departments as shown in (Table 1). Further, software and equipment used for analysis, modeling and data collection are shown in Table 2 below.

Table 2. Software and equipment used in the study

Application/Instrument	Type	Task
ArcGIS v.10.4	Software	Digital image processing and analysis, GIS analysis and mapping
ERDAS Imagine v.2014	Software	Digital image processing
Handheld GPS (Nomad 900 Series)	Equipment	Picking coordinates, locating points and mapping
Probing Thermometer	Equipment	*In-situ* ground surface temperature measurements

To retrieve land surface temperature and the subsequent identification of surface thermal anomalies associated with geothermal features in a known geothermal area, single channel and split window algorithms were employed. Single channel methods require only a single thermal infrared band to retrieve LST while split window methods use two thermal infrared bands in the atmospheric window. Both Landsat Thematic Mapper (TM) and Enhanced Thematic Mapper Plus (ETM+) have a single thermal band (i.e. band 6) while Landsat 8 has two thermal bands (band 10 and 11). Thematic Mapper represents Landsat 4 and 5, while ETM+ is Landsat 7. Thus, whereas single channel methods and algorithms can be used with any Landsat data that has at least one thermal infrared band, split window methods can only be used with Landsat 8 due to presence of two thermal infrared (TIR) bands in the atmospheric window.

C. Split window method

The basis for split window approach is that radiance attenuation for atmospheric absorption is proportional to the radiance difference of

simultaneous measurements at two different wavelengths, each wavelength being subjected to different amounts of atmospheric absorption. Landsat 8 TIRS bands (band 10 and 11) were designed to allow the use of split window algorithms for atmospheric correction and land surface temperature retrieval [17]. The use of two separate and relatively narrow thermal bands in LST retrieval has been shown to produce reliable results through minimization of retrieval errors [23].

The flow chart diagram (Fig. 2) shows the approach adopted for LST retrieval using split window method.

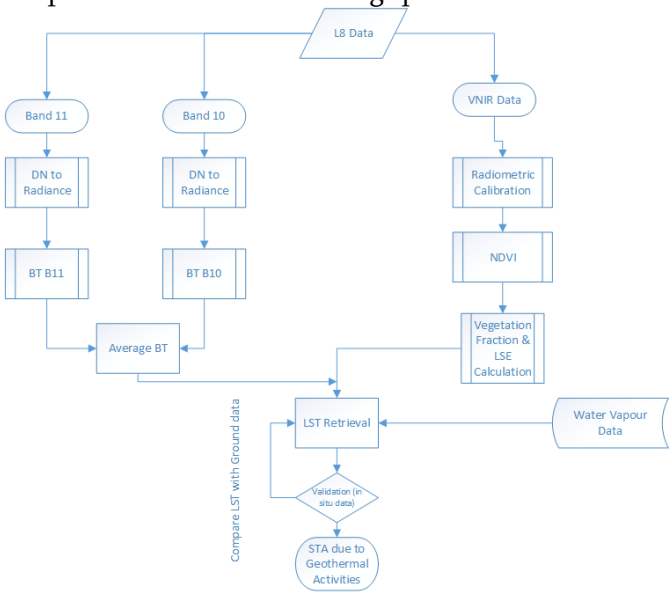

Fig. 2 Steps followed in LST retrieval using split window method

Landsat 8 level-1 data product was the primary data source. Both L8 TIRS band 10 and 11 raw data in quantized and calibrated scaled digital numbers (DN) were converted to Top of Atmosphere (TOA) spectral radiance (1) and at-satellite Brightness Temperature (BT) in °C (2) using DNs to physical units conversion formulas (equation (1) and (2)) provided by [17]. Radiometric rescaling coefficients values provided in the data metadata files were also used.

$$L_\lambda = M_L * Q_{cal} + A_L \quad (1)$$

Where

L_λ is top of atmosphere (TOA) spectra radiance in (watts/m²*srad*μm), M_L is band's radiance multiplicative scaling factor, A_L is band's radiance additive scaling factor, and Q_{cal} is quantized and calibrated standard pixel values in DN (Level-1 product image). Both multiplicative (i.e. Radiance Mult_Band) and additive (i.e. Radiance Add_Band) scaling factors (Table 3) are given in Landsat-8 Level-1 product metadata file.

Table 3. Landsat-8 rescaling factors and thermal constants values from metadata file (MTL.txt)

	Factor	Band 10	Band 11
Rescaling Factors	Radiance Mult_Band	3.3420E-04	3.3420E-04
	Radiance Add_Band	0.10000	0.10000
Thermal Constants	K1	774.8853	480.8883
	K2	1321.0789	1201.1442

$$T = \frac{K_2}{ln\left(\frac{K_1}{L_\lambda} + 1\right)} - 273.15 \quad (2)$$

Where T is at-satellite brightness temperature (BT) in °C, L_λ is TOA spectral radiance, K_1 and K_2 are thermal conversion constants (Table 3) from metadata file.

Landsat-8 OLI visible and near infrared (VISNIR) bands were checked for radiometric calibration errors against Landsat 7 data of the study areas and were found to be soundly calibrated radiometrically. Near infrared (band 5) and visible red band (band 4) were used to compute Normalized Difference Vegetation Index (NDVI) of the study area.

$$NDVI = \frac{(NIR - Red)}{(NIR + Red)}$$

Thus, for Landsat 8 data, NDVI was calculated as below;

$$NDVI = \frac{(Band\ 5 - Band\ 4)}{(Band\ 5 + Band\ 4)}$$

Fractional Vegetation Cover (FVC) also referred to as proportion of vegetation cover was calculated form NDVI results as shown below:

$$FVC = \left(\frac{NDVI - NDVI_{min}}{NDVI_{max} - NDVI_{min}}\right)^2$$

Where:

FVC – Fractional Vegetation Cover
NDVI – Normalized Difference Vegetation Index

$NDVI_{max}$ – Maximum of NDVI
$NDVI_{min}$- Minimum of NDVI

Land surface emissivity (LSE) of the study area was estimated using NDVI Threshold method. The generated LSE values for band 10 and 11 were used to calculate the mean and difference LSE values of the study area.

$$LSE = \varepsilon_s(1 - FVC) + \varepsilon_v * FVC \quad (3)$$

Where ε_s is soil emissivity, ε_v is vegetation emissivity, and FVC is fractional vegetation cover.

Table 4. Soil and Vegetation Emissivity Values for L8 TIRS Bands

TIRS Band	Soil emissivity (ε_s)	Vegetation emissivity (ε_v)
Band 10	0.9668	0.9863
Band 11	0.9747	0.9896

D. Water vapor content

The atmospheric water vapor content in g/cm² of the study area was supposed to be obtained at the time of Landsat-8 data acquisition. However, absence of a meteorological station in the study area necessitated the use of water vapor data from MODIS water vapor products: MOD05_L2. MODIS data used was acquired on the same date as Landsat 8 data (i.e. July 31, 2018). Using the scale factor of 0.001 and add-offset value of 0 (from MODIS MOD05_L2 metadata file), MOD05_L2 water vapor product with a spatial resolution of approximately 1 km was converted into water vapor content in g/cm². However, for easier integration of water vapor data with Landsat-8 data, derived water vapor content from MODIS was resampled to 30 m spatial resolution.

In this study, the split window algorithm presented by [1] was adopted.

$$LST = BT_{10} + C_1(BT_{10} - BT_{11}) + C_2(BT_{10} - B_{11})^2 + C_0 + (C_3 + C_4W)(1 - \varepsilon) + (C_5 + C_6W)\Delta\varepsilon \quad (4)$$

Where LST is land surface temperature in °C, BT_{10} and BT_{11} are band 10 and 11 brightness temperature respectively, C_0 - C_6 are coefficient values for the split window algorithm (Table 5), ε is mean land surface emissivity (LSE) of Landsat-8 TIRS bands; $(\varepsilon_{10} + \varepsilon_{11}) \div 2$, $\Delta\varepsilon$ is TIRS bands LSE difference, W is water vapor content, ε_{10} *and* ε_{11} are LSE of band 10 and 11 respectively

Split window coefficient values

Table 5. Split window coefficient values adopted from [23]

Coefficient	C_0	C_1	C_2	C_3	C_4	C_5	C_6
Value	-0.268	1.378	0.183	54.300	-2.238	-129.200	16.400

E. Single channel method

This method requires only a single thermal band to retrieve land surface temperature. Landsat 8 TIRS band 10 was used. Further, a single channel algorithm presented by [24] was adopted in this study due to its simplicity and minimal input parameters in LST retrieval. However, other forms of single channel methods and algorithms exist e.g. single channel and the generalized single channel method [1], [13], [19], [25] and the mono-window algorithm [18], [26]. The flow chart diagram (Fig. 3) outlines the approach used to retrieve LST using single channel method

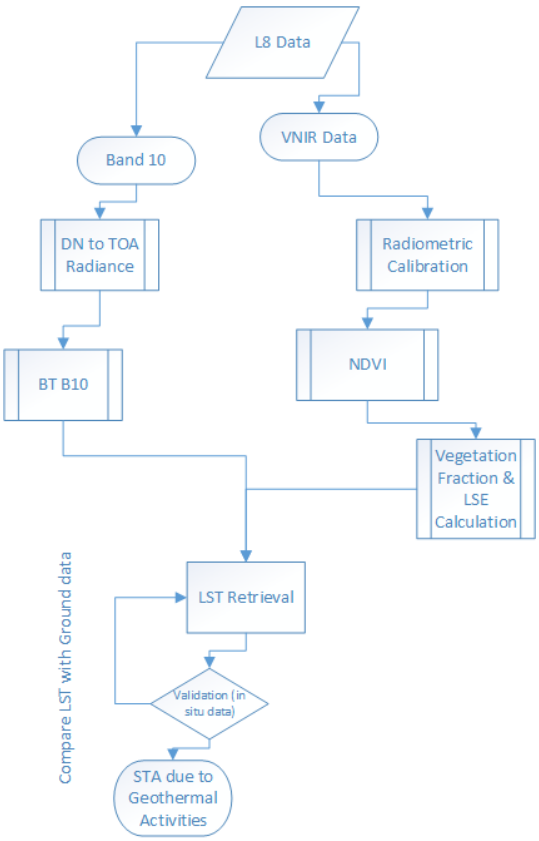

Fig. 3. Steps followed in LST retrieval using single channel method

The steps followed were as explained under the split window approach only that for the adopted single channel method, a single thermal band was used and no water vapor content data was required, equation (5).

Single channel algorithm for retrieving LST

$$T_s = \frac{T_{sensor}}{1 + \left(\lambda * \frac{T_{sensor}}{\rho}\right) ln\, \varepsilon} \quad (5)$$

Where T_s is land surface temperature in °C, λ is wavelength of the emitted radiance, $\rho = h * \frac{c}{\sigma}$ in mK where;

$h = 6.626 * 10^{-34} Js$ (Planck's constant)

$c = 2.998 * 10^{8}\ m/s$ (Velocity of light)

$\sigma = 1.38 * 10^{-23}\ J/K$ (Boltzmann constant)

T_{sensor} is at-sensor brightness temperature (BT) in °C given by:

$$T_{sensor} = \frac{K_2}{\ln\left(\frac{K_1}{L_\lambda} + 1\right)} - 273.15$$

The meaning of input parameters are as discussed in previous equations.

To validate retrieved Land Surface Temperature from both split window and single channel algorithm, comparison was made with *in-situ* ground surface temperature measurements carried out in the study area (i.e. known geothermal area). This comparison was meant to identity the better LST retrieval method between split window and single channel method using Landsat-8 data. Ground surface temperature of the sampled validation points of the study area were measured using a probing thermometer (with a temperature range of -50.0°C to 150.0°C) while handheld GPS (Nomad 900 Series from Trimble) was used to record coordinates of the validation points.

Through validation, comparison, and identification of the best retrieved LST output, surface characterization of the study area followed by analysis with existing geothermal information and ground truth surveys to identify surface thermal anomalies associated with geothermal features. The characteristics and features of the identified thermal anomalies from a known geothermal area were later used to characterize and identify surface thermal anomalies associated with geothermal features in a geothermal prospect area; Baringo County.

III. RESULTS AND DISCUSSION

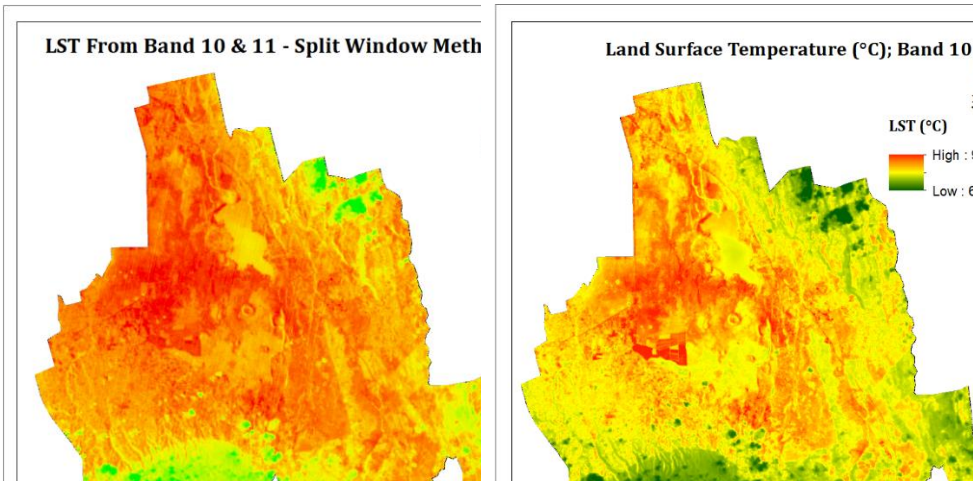

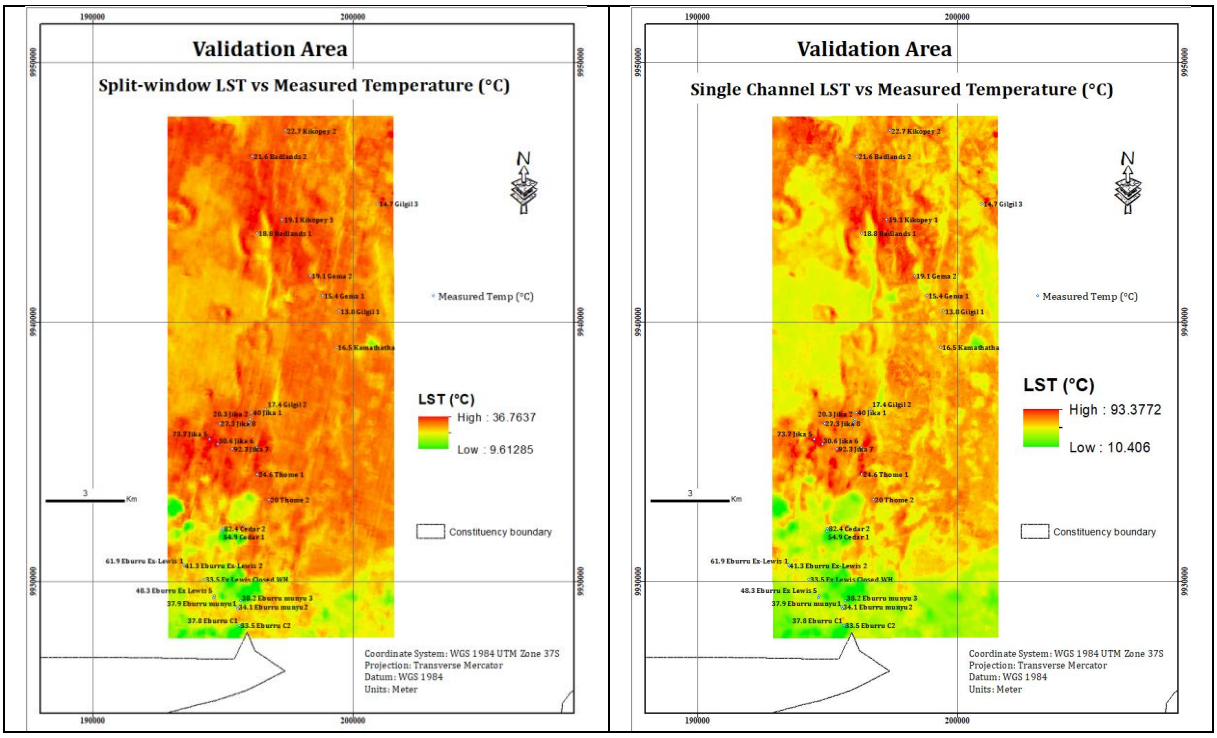

Fig. 4 Land surface temperature (LST) as retrieved by split window method (top left) and by single channel method (top right). Bottom figures shows an overlay of LST and in-situ measured temperature over validation area; split window method (bottom left) and single channel method (bottom right)

Land surface temperature outputs by both single channel and split window algorithm employed in this study against the field measured ground temperature of the validation area were compared visually and statistically. Visual inspection of LST outputs overlain by *in-situ* field temperature values (Fig. 4) shows that surface thermal anomalies were more clearly defined and identifiable under single channel derived LST map (Fig. 4, top right) compared to those under LST map derived by split window algorithm (Fig. 4, top left).

To compare the outputs statistically, a representative observation points from the field validation exercise were selected from the total measured points. The selected points represented areas observed during validation fieldwork to have surface geothermal manifestations such as fumaroles, steaming hot grounds and hydrothermally altered grounds, and those without surface geothermal manifestations. Further, these were the only observations done on the day of satellite overpass. The observed temperature of these representative field points were then compared with the estimated temperature from both single channel (Table 6) and split window method (7).

Table 6. Single channel estimated temperature against observed temperature

Point Name	Estimated Temp (°C)	Observed Temp (°C)	Residual Squared	
Eburru Ex-Lewis 1	28.64	61.9	1106.2276	
Cedar 1	16.48	54.9	1476.0964	r = 0.8535942
Thome 5	47.57	88.4	1667.0889	r^2 = 0.728623
Jika 7	46.46	92.3	2101.3056	RMSE = 20.500271
Cedar 2	26.25	82.4	3152.8225	

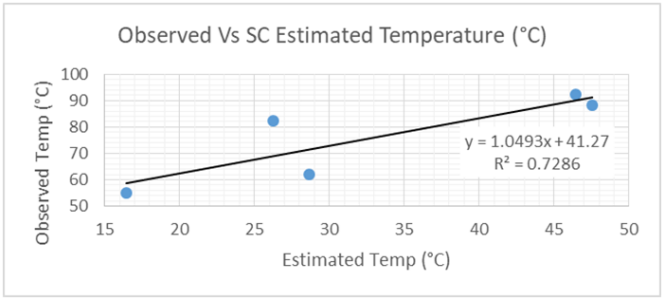

Fig. 5. Scatter plot and regression values for Table 6

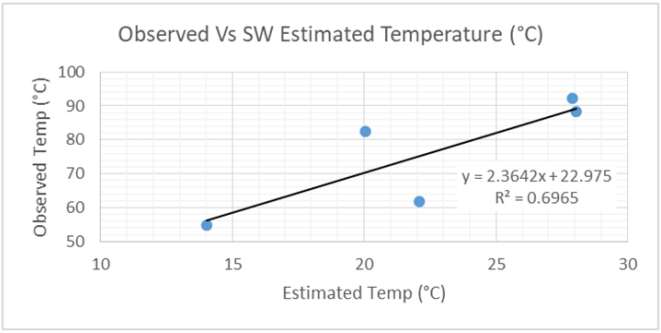

Fig. 6. Scatter plot and regression values for Table 7

Table 7. Split window estimated temperature against observed temperature

Point Name	Estimated Temp (°C)	Observed Temp (°C)	Residual Squared	
Eburru Ex-Lewis 1	22.1	61.9	1584.04	
Cedar 1	14.02	54.9	1671.1744	r = 0.8345726
Thome 5	28.03	88.4	3644.5369	r^2 = 0.6965115
Jika 7	27.89	92.3	3886.2756	RMSE = 26.998285
Cedar 2	20.06	82.4	4148.6481	

From the comparison tables (Table 6 & Table 7) and scatter plots (Fig. 5 & Fig. 6), both methods had strong positive correlation coefficient against observed ground temperatures. However, single channel method output had a stronger correlation coefficient of 0.85 compared to 0.83 of split window method. Further, single channel method had a lower root mean square error (RMSE) compared to that of split window output. This means that LST output by single channel method when compared against in-situ observed temperatures, had better concentration of data around the line of best fit while split window had more spread out data around the line of best fit. The spatial distribution of sampled derived LST and field measured points both with a wide temperature range and presence of outlier values led to high values of RMSE in both cases.

Therefore, from the outlined comparison; visual and statistical, single channel method gave better results compared to split window method. Surface thermal anomalies are clearly defined on land surface temperature map derived by single channel method and there is a strong positive correlation coefficient between estimated temperature values and the in-situ ground measured temperature. According to [17] there exist large calibration uncertainty associated with Landsat 8 TIRS band 11 due to errors caused by stray light and therefore recommends users to refrain from relying on band 11 data in quantitative analysis of thermal infrared sensor data. Split window techniques require two thermal bands to retrieve land surface temperature and under the present study, Landsat 8 TIRS band 10 and 11 were used. Hence, the use of band 11 might have affected the retrieved LST by split window method leaving LST retrieved by single channel method a better result.

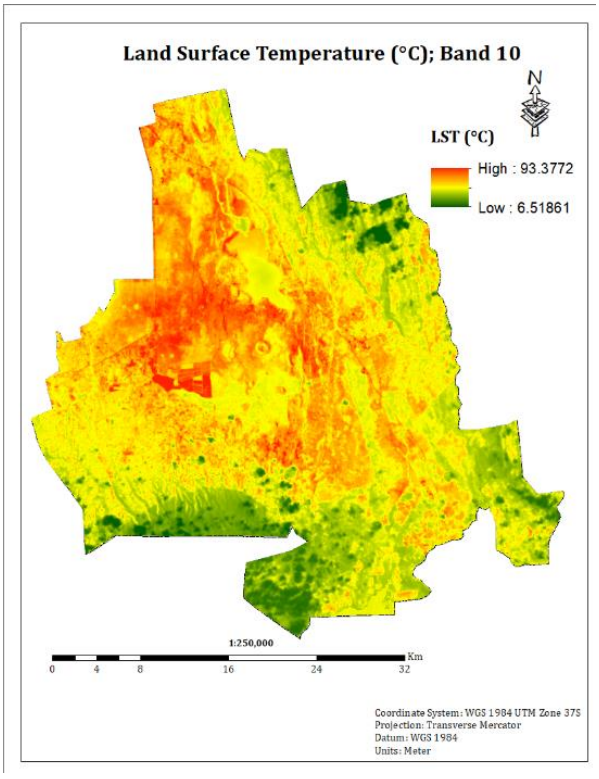

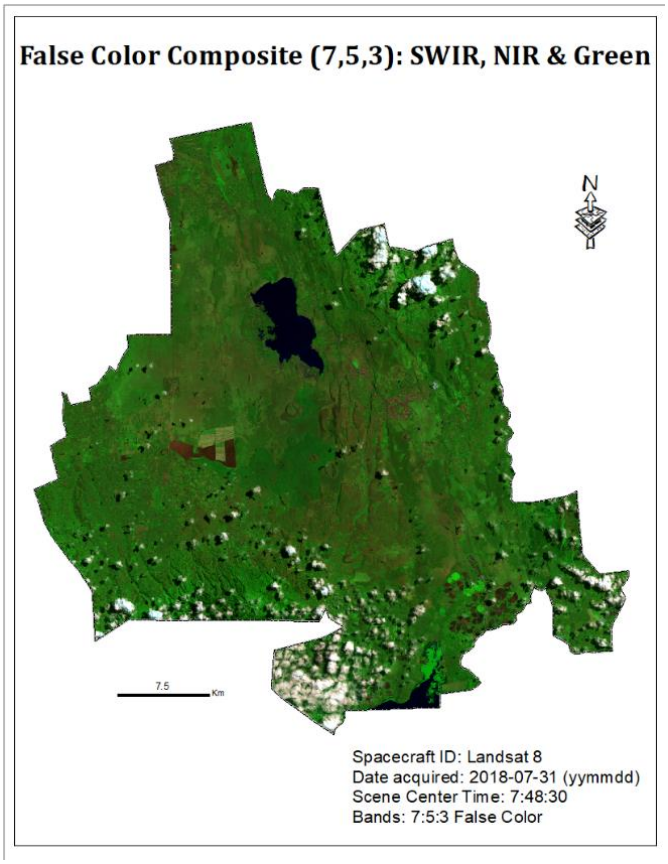

Fig. 7 Land surface temperature map of known geothermal study area retrieved using single channel method (left figure) and natural composite image (i.e. Landsat-8 bands 7, 5, 3) of the study area for visual comparison (right figure)

Compared to land surface temperature derived using split-window algorithm (Fig. 4 top left and bottom left figures), single channel derived LST maps had better defined temperature zones and clearly defined surface thermal anomalous areas within the study area (Fig. 4 top right and bottom right figures & Fig. 7 left figure). The highest derived temperature was 93.38 °C while the lowest was 6.52 °C. The western region of the study area excluding bare soil of the ploughed agricultural farm – triangular shaped feature – as seen in (Fig. 7 right figure), central area, and mid-southern part of the study area had the highest land surface temperature (red colored regions). The dominance of yellow color on temperature map indicate that most of the areas within the study area had medium temperature that can be regarded as normal background temperature. Water bodies had a slightly lower temperature compared to normal background temperature. However, forested areas and cloud-covered pixels recorded the lowest derived temperature (Fig. 7).

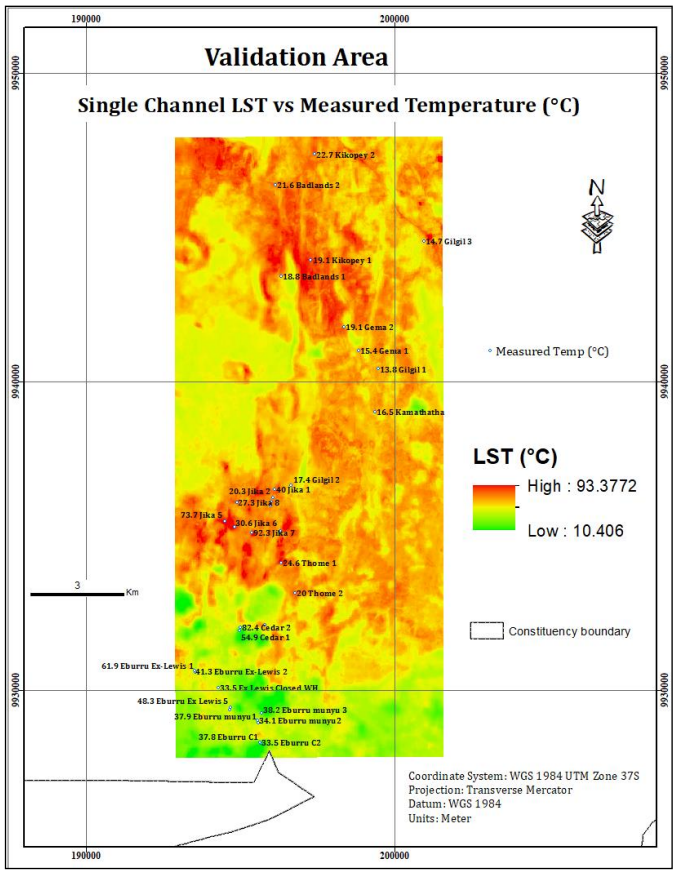

Fig. 8 An overlay of in-situ measured ground temperature over single channel retrieved LST within the validation area

By considering the defined validation area, comparison of single-channel derived temperature and field measured temperature shows the closeness of the two set of temperature values. The highest temperature derived was 93.38 °C while that measured in the field was 92.3 °C at Jika 7 which happens to be over a thermal anomaly area (Fig. 8). On the other hand, 10.41 °C was the lowest derived temperature within the validation area while 13.8 °C at *Gilgil 1* was the lowest ground measured temperature. This lowest measured ground temperature along with other low temperature measured points especially in the eastern and north-eastern part of the validation area occur over areas mapped as having medium temperature (Fig. 8).

The different versions of single channel algorithms and methods of deriving land surface temperature requires only a single thermal band [1], [19]. The method has been widely used in land surface temperature mapping for a variety of applications including detection of thermal anomalies associated

with geothermal systems and in environmental studies [9], [14], [16], [27].

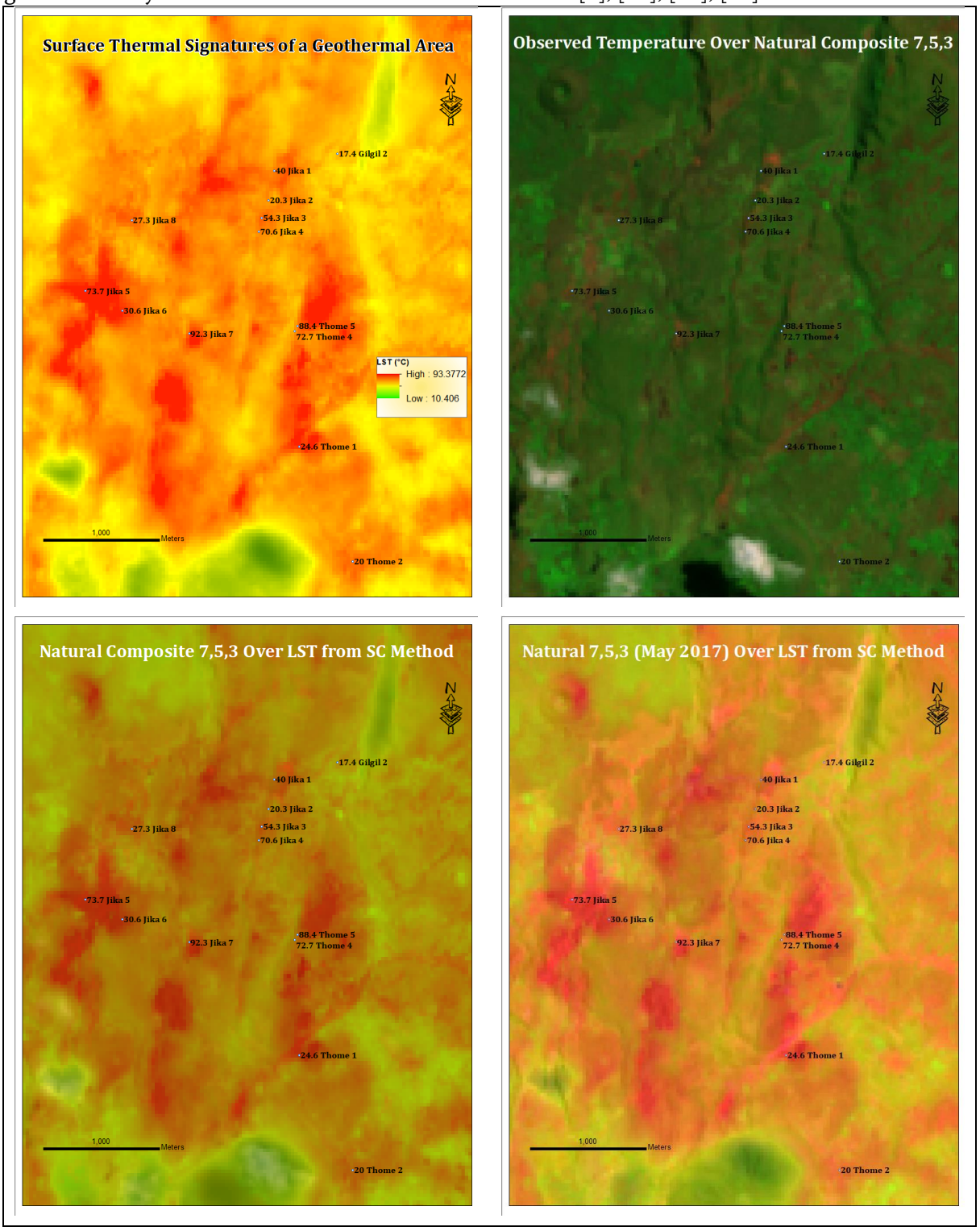

Fig. 9 Detection and identification of thermal anomalies and signatures associated with surface geothermal manifestation features and systems in a known geothermal area.

In (Fig. 9) top left figure shows surface thermal anomalies (red spots) on a retrieved land surface temperature map of Eburru-Jika; a known geothermal area. Top right, field measured temperature values are overlain on a false color natural composite (bands 7, 5, 3) of the Eburru-Jika geothermal area. Bottom left, an overlay of natural composite (bands 7, 5, 3) over land surface temperature retrieved using single channel method. Bottom right figure, an overlay of natural composite (7, 5, 3) from May 25th 2017 Landsat-8 data over retrieved land surface temperature.

According to [28], surface thermal anomalies are elevated surface temperature above the normal

background surface temperature that give rise to localized heat islands or heat anomalies. Surface geothermal manifestation features such as fumaroles, hot springs, geysers, mud pools and hot grounds have elevated temperatures above their surroundings and are thus easily identified as thermal anomalies from thermal infrared data. Thermal anomalies (Fig. 9, top left) are clearly defined and distinguishable (red color) from the normal surface temperature (different shades of yellow) dominant over the land surface temperature map. The highest retrieved LST for an individual pixel was 93.38°C while the lowest was 10.41°C. This shows that surface thermal anomalies associated with geothermal activities and especially in very active geothermal regions, might have very high ground temperature e.g. 92.3°C recorded for Jika 7 (Fig. 9 top left map & Fig. 8).

By overlaying retrieved land surface temperature of a known geothermal area with natural composite images and field measured temperature values (Fig. 9, top right, bottom left and right figures), this study endeavored to highlight how to detect, identify and delineate surface thermal anomalies and subsequently surface thermal signatures associated with geothermal features and systems in a known geothermal area. The identified signatures would then be used in an area prospected to have geothermal surface manifestations and resources as a tool to aid further exploration. The main geothermal surface signature identified by the current study was high temperature surface thermal anomalies from the retrieved LST maps.

With single channel method giving superior results in land surface temperature mapping and subsequent identification of thermal anomalies associated with geothermal features compared to split window algorithm and taking into consideration the caution given against the use of Landsat 8 TIRS band 11 data due to effects of stray light [17], only single channel method was used in LST mapping and identification of geothermal features based on thermal anomalies in the second study area; Baringo County, in Kenya.

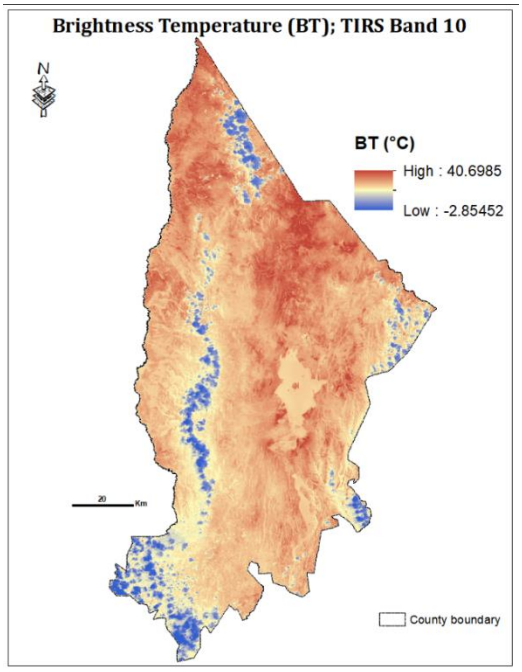

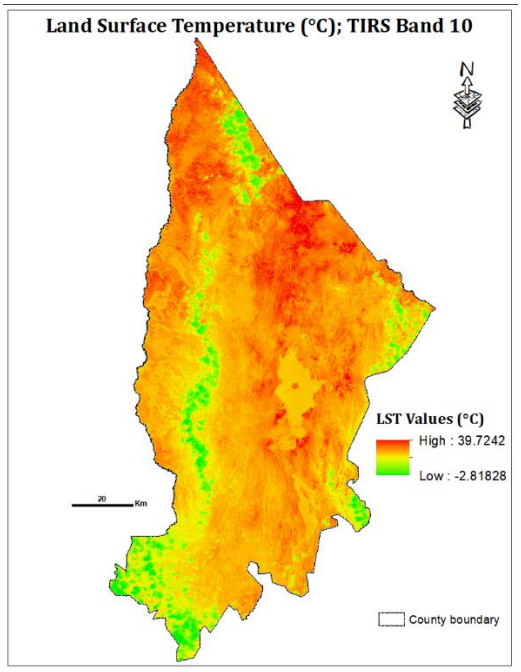

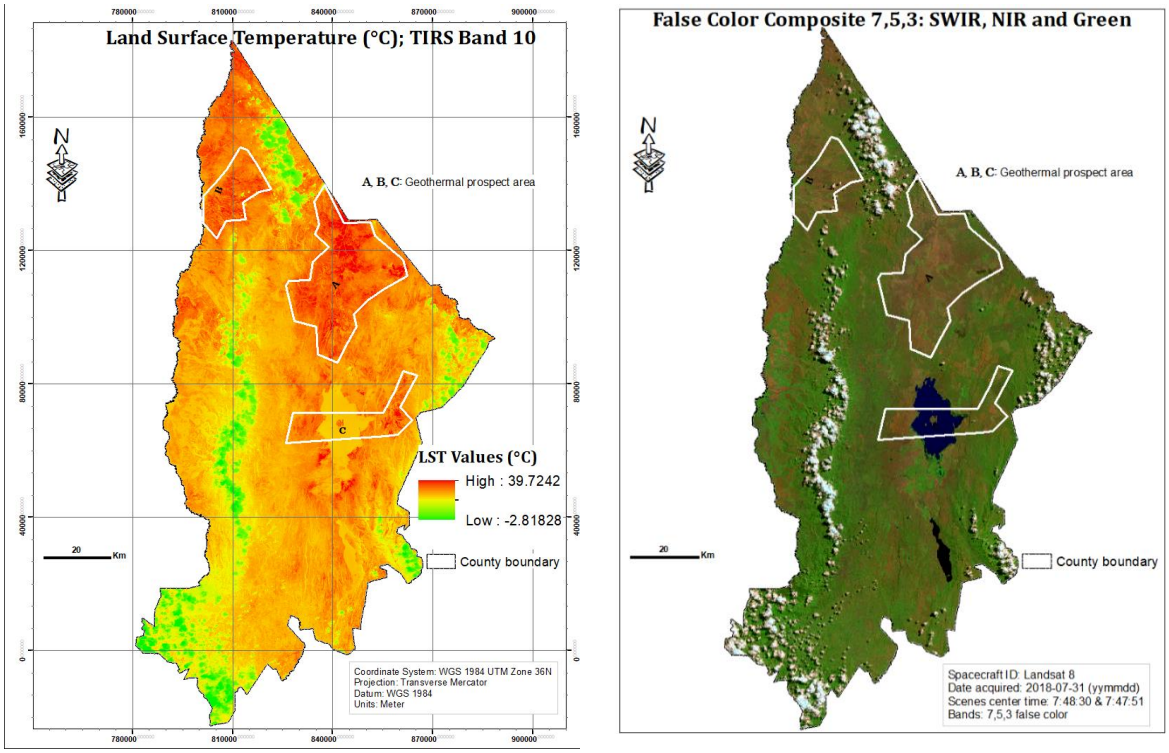

Fig. 10 Second study area surface characterization. At-sensor brightness temperature (top left), LST in °C (top right and bottom left), and natural composite image (bottom right)

In (Fig. 10), top left figure is at-sensor brightness temperature map of Baringo County. Top right is land surface temperature as derived using single channel method. Bottom left is LST map but with geographical grids included. Finally, bottom right is natural color composite (bands 7, 5, 3 of L8) image of the study area. The bottom figures of (Fig. 10) are shown in details in (Fig. 11 & Fig. 12)

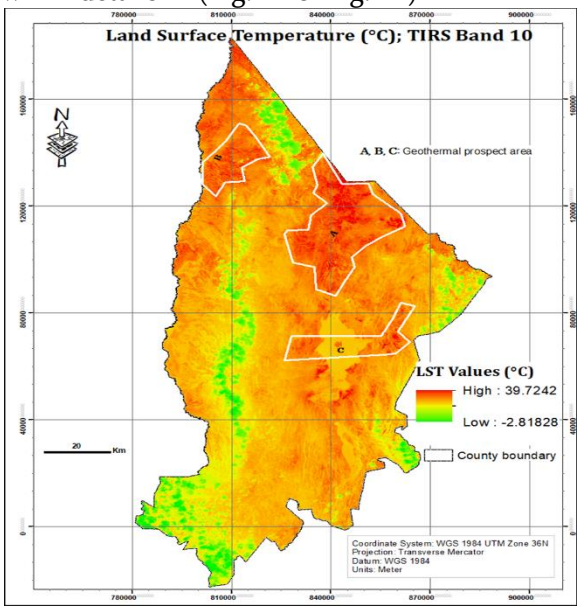

Fig. 11. Land surface temperature and three identified geothermal prospect areas namely: A, B, and C

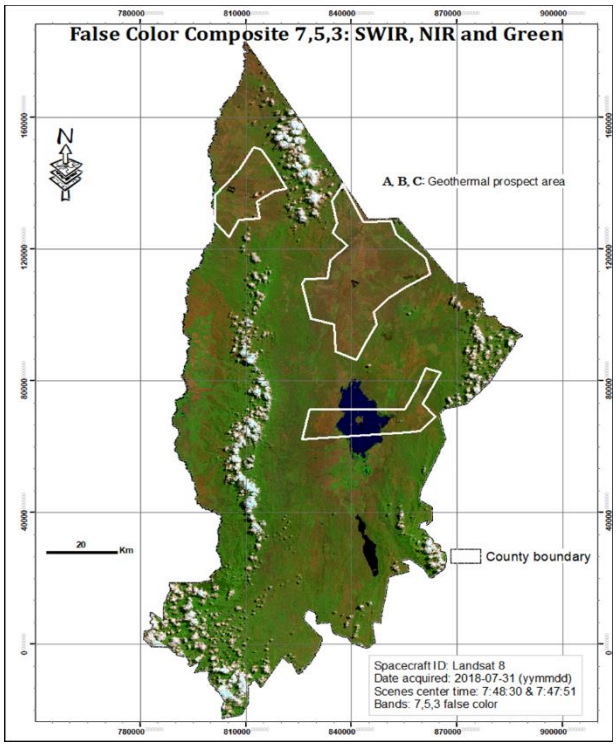

Fig. 12 False color natural composite of Landsat-8 bands (7, 5, 3); shortwave infrared, near infrared and green overlain by three identified geothermal prospects

For the second study area; Baringo County, land surface temperature map (Fig. 11) was the main result. The highest derived temperature was 39.72 °C and the lowest was -2.82 °C. The negative temperature values

were due to presence of clouds (green color in the LST map) in the satellite imagery. Higher temperatures were recorded in the north, north-eastern and areas around Lake Baringo as characterized by dense red color. Most of the other areas within the study area had medium level temperature (different shades of yellow in Fig.11) while water bodies recorded lower temperature. Negative temperature values of cloud-covered pixels were not taken into consideration but rather considered as noise.

By characterizing the study area in terms of surface temperature (Fig. 11), a number of surface thermal anomalies were identified from which three geothermal prospect areas (A, B, and C) were suggested (Fig.11 & Fig. 12). Surface thermal anomalies are said to be elevated surface temperature above the normal or background surface temperature thereby giving rise to localized heat islands [28]. The approach of land surface characterization through surface temperature mapping, detection and monitoring of surface thermal anomalies associated with geothermal features and resources has been widely used as a tool in geothermal exploration [5], [6], [8], [9], [29]–[31].

According to [22], [32] geological, geochemistry, and geophysical studies especially resistivity measurements, and surface geothermal manifestations at Lake Baringo, Korosi, Chepchuk volcanic field, and Paka have proved existence of geothermal resources in the prospects. The resource temperature of the identified prospects range from intermediate suitable for direct uses in Lake Baringo to high temperature geothermal resource at Korosi prospect suitable for power generation. The enumerated prospects coincide with the identified and suggested geothermal prospects A and C (Fig. 11 & Fig. 12). Prospect A represents Korosi, Chepchuk, and Paka geothermal prospects. Prospect B apparently seems new and thus, this study recommends further investigations to confirm presence of surface manifestations and geothermal resources. Finally, prospect C represents Lake Baringo prospect which according to [22], potential fault-controlled discrete geothermal reservoirs occur in areas west of the lake, south-eastern and northern region.

The successful use of both split window and single channel method to detect, identify, delineate and finally map surface thermal anomalies associated with geothermal features demonstrate the importance of satellite remote sensing data (i.e. Landsat-8 data) and techniques in exploring for geothermal resources. Although the two methods employed in this study had different levels of accuracy in LST retrieval and detection of surface thermal anomalies, both gave valuable results that would complement conventional geothermal exploration surveys. Through the two methods, land surface temperature maps and the resultant surface thermal anomalies of known geothermal area (Fig. 4) were successfully retrieved. Using the identified thermal signatures from the retrieved LST and field validation data of known geothermal area, land surface temperature and surface thermal anomalies of a geothermal prospect area were retrieved using single channel method (Fig. 11). By producing better result compared to split window method, single channel method was preferred in retrieving LST of a geothermal prospect (Baringo County) that has not been fully confirmed as geothermal area.

This demonstrates how satellite remote sensing can be used as a cost-effective tool to enhance exploration of known and unknown large geothermal areas for geothermal potential and subsequently identification of specific targets for detailed and comprehensive exploration investigations using higher resolution methods such as ground based surveys, airborne, or drones' surveys. Further, analysis of surface thermal anomalies maps alongside geological, geophysical and geochemical information provides comprehensive picture of known geothermal areas and can help extend known fields as well as discovery of new geothermal resource areas.

Both split window and single channel methods were applied in this study to derive land surface temperature from thermal infrared bands of Landsat 8 data. Validation field work of *in-situ* ground temperature measurements was carried out on the day of satellite passage over the known geothermal area as well as a few days before and after the satellite passage due to the large geographical extent of the study area. Analysis of the derived LST maps, thermal anomalies, *in-situ* ground data, and existing

geothermal information of the region of interest, led to delineation of surface thermal anomalies associated with geothermal features in a known geothermal area; Gilgil district comprising of Eburru-Jika-Badlands-Elementaita geothermal areas. With single channel method giving superior results in a known geothermal area, it was applied in the second study area; Baringo County, a geothermal prospect area. Analysis of the derived LST and detected surface thermal anomalies with existing geothermal exploration information, and different image composites of the area led to identification of 3 geothermal prospect areas namely A, B, and C that were recommended for detailed geothermal investigations.

Detection of surface thermal anomalies associated with geothermal features and subsequent identification of geothermal prospects for detailed exploration investigations using higher resolution methods e.g. ground surveys or airborne remote sensing, demonstrates the power of satellite remote sensing data and techniques in enhancing geothermal exploration activities. Landsat 8 satellite remote sensing data is public domain and free access data provided by United States Geological Survey (USGS). Its relatively high spatial resolution (30 m for visible, near infrared and short wave infrared bands, and 100 m resampled to 30 m for long wave infrared TIRS bands), temporal resolution of 16 days, and good spectral and radiometric resolutions offers a cost-effective means for exploring geothermal areas. Further, it allows large areal coverage and gives immediate results. Therefore, the use of free access and available satellite remote sensing data should be encouraged as support tool in surface geothermal exploration activities.

This study therefore demonstrates the cost-effectiveness of satellite remote sensing data, in this case public domain and free-access Landsat-8 data, and techniques in exploring large areas for geothermal potential through surface temperature mapping, and detection of surface thermal anomalies associated with geothermal features and resources. Subsequently smaller targets were identified for further and high resolution investigations that may result to expansion of existing geothermal areas, and discovery of new geothermal potential areas.

IV.RECOMMENDATIONS

To enhance the quality of retrieved land surface temperature maps and surface thermal anomalies, validation field work of *in-situ* temperature measurements should be carried out on a clear day of satellite passage at multiple points within the study area. This will eliminate errors due to temporal variation of atmospheric conditions for measurements done on multiple days. Forward looking infrared camera (FLIR) if available can be used instead of a probing thermometer for surface temperature measurement. FLIR has a relatively large areal coverage compared to L8 TIRS 30 m spatial resolution (resampled from 100 m) while probing thermometer (used in this study) only gives point values. The choice of a cloudless satellite passage day will eliminate presence of clouds in satellite imagery and hence mitigation of artifacts associated with cloud and cloud shadows.

To enhance surface thermal anomalies detection and monitoring from satellite remote sensing data (e.g. Landsat 8 TIRS) in geothermal environments, future work should focus on reducing noise from background emittances and non-geothermal thermal emittances such as human activities. Thus, corrections for topographic slope aspect, thermal inertia, albedo, and solar and elevation effects are highly recommended. These corrections have been shown to increase the number of identified thermal anomalies and also distinguishes geothermal-based anomalies from false anomalies.

From previous works and existing literature, use of two thermal bands in the atmospheric window for retrieval of surface temperature values using split window methods gave better results compared to the use of only one thermal band under single channel methods. However, under the current study using Landsat 8 TIRS data, single channel retrieved LST was more accurate than split window retrieved LST when compared to validation data from *in-situ* ground temperature data. Single channel method used TIRS Band 10 only while split window method used both TIRS bands; Band 10 and 11. However, Band 11 has been identified to have large calibration uncertainty due to errors caused by stray light, and as a result, affects the output of split window. Thus, until the

discovered stray light issues are corrected and Landsat 8 TIRS data is reprocessed, this study recommends the use of TIRS Band 10 only in retrieval of land surface temperature.

Through successful retrieval of land surface temperature, identification and delineation of surface thermal anomalies associated with geothermal resources, satellite remote sensing data and techniques ought to be integrated into geothermal exploration activities as support tool to enhance surface investigations for geothermal resources.

V. ACKNOWLEDGMENT

Authors duly appreciate data available from the U.S. Geological Survey and data distributed by the Land Processes Distributed Active Archive Center (LP DAAC), located at USGS/EROS, Sioux Falls, SD. http://lpdaac.usgs.gov

Conflict of Interest

The author declares that there is no conflict of interests regarding the publication of this paper.

VI. REFERENCES

[1]. J. C. Jiménez-Muñoz, J. A. Sobrino, D. Skokovi´, C. Mattar, and J. Cristóbal, "Land surface temperature retrieval methods from Landsat-8 thermal infrared sensor data," Geosci. Remote Sens. Lett. IEEE, vol. 11, no. 10, pp. 1840–1843, 2014.

[2]. O. Rozenstein, Z. Qin, Y. Derimian, and A. Karnieli, "Derivation of Land Surface Temperature for Landsat-8 TIRS Using a Split Window Algorithm," Sensors (Switzerland), vol. 14, no. 4, pp. 5768–5780, 2014.

[3]. T. Zhang et al., "Estimation of the Total Atmospheric Water Vapor Content and Land Surface Temperature Based on AATSR Thermal Data," Sensors, vol. 8, no. 3, pp. 1832–1845, 2008.

[4]. Z. L. Li et al., "Satellite-derived land surface temperature: Current status and perspectives," Remote Sens. Environ., vol. 131, pp. 14–37, 2013.

[5]. J. Mutua and G. Mibei, "Remote Sensing Application in Geothermal Exploration: Case Study of Barrier Volcanic Complex, Kenya," GRC Trans., vol. 35, pp. 943–947, 2011.

[6]. F. M. Howari, "Prospecting for geothermal energy through satellite based thermal data : Review and the way forward," Glob. J. Environ. Sci. Manag., vol. 1, no. 4, pp. 265–274, 2015.

[7]. W. M. Calvin, M. Coolbaugh, and C. Kratt, "Application of remote sensing technology to geothermal exploration," Geol. Surv. …, no. May, pp. 1083–1089, 2005.

[8]. M. F. Coolbaugh, C. Kratt, A. Fallacaro, W. M. Calvin, and J. V. Taranik, "Detection of geothermal anomalies using Advanced Spaceborne Thermal Emission and Reflection Radiometer (ASTER) thermal infrared images at Bradys Hot Springs, Nevada, USA," Remote Sens. Environ., vol. 106, no. 3, pp. 350–359, 2007.

[9]. M. Eneva, M. Coolbaugh, S. C. Bjornstad, J. Combs, C. Westchester, and S. Diego, "In Search for Thermal Anomalies in the Coso Geothermal Field (California) using Remote Sensing and Field Data," in Geothermal Reservoir Engineering, 2007.

[10]. S. Karki, S. K. Nawotniak, H. C. Bottenberg, M. Mccurry, and J. Welhan, "Determination of Geothermal Anomalies Through Multivariate Regression of Background Variables at Yellowstone National Park Using Landsat 5 TM Thermal Band Data," vol. 38, 2014.

[11]. M. Eneva and M. F. Coolbaugh, "Importance of elevation and temperature inversions for the interpretation of thermal infrared satellite images used in geothermal exploration," GRC Trans., vol. 33, pp. 467–470, 2009.

[12]. J. C. Jimenez-Munoz, J. Cristobal, J. A. Sobrino, G. Sòria, M. Ninyerola, and X. Pons, "Revision of the single-channel algorithm for land surface temperature retrieval from landsat thermal-infrared data," IEEE Trans. Geosci. Remote Sens., vol. 47, no. 1, pp. 339–349, 2009.

[13]. J. C. Jiménez-Muñoz and J. A. Sobrino, "A single-channel algorithm for land-surface temperature retrieval from ASTER data," IEEE Geosci. Remote Sens. Lett., vol. 7, no. 1, pp. 176–179, 2010.

[14]. Z. Zhang et al., "Towards an operational method for land surface temperature retrieval from Landsat 8 data," Remote Sens. Lett., vol. 7, no. 3, pp. 279–288, 2016.

[15]. C. Du, H. Ren, Q. Qin, J. Meng, and J. Li, "Split-Window algorithm for estimating land surface temperature from Landsat 8 TIRS data," Int. Geosci. Remote Sens. Symp., no. Ldcm, pp. 3578–3581, 2014.

[16]. U. Avdan and G. Jovanovska, "Algorithm for automated mapping of land surface temperature using LANDSAT 8 satellite data," J. Sensors, vol. 2016, pp. 1–8, 2016.

[17]. USGS and NASA, Landsat 8 Data Users Handbook, vol. 2. Sioux Falls, 2016.

[18]. F. Wang, Z. Qin, C. Song, L. Tu, A. Karnieli, and S. Zhao, "An Improved Mono-Window Algorithm for Land Surface Temperature Retrieval from Landsat 8 Thermal Infrared Sensor Data," Remote Sens., vol. 7, no. 4, pp. 4268–4289, 2015.

[19]. J. A. Sobrino, J. C. Jiménez-Muñoz, and L. Paolini, "Land surface temperature retrieval from LANDSAT TM 5," Remote Sens. Environ., vol. 90, no. 4, pp. 434–440, 2004.

[20]. M. F. Coolbaugh, J. V. Taranik, and F. A. Kruse, "Mapping of surface geothermal anomalies at Steamboat Springs, NV using NASA Thermal Infrared Multispectral Scanner (TIMS) and Advanced Visible and Infrared Imaging Spectrometer (AVIRIS) data," Proceedings, 14th Themat. Conf. Appl. Geol. Remote Sens., pp. 623–630, 2000.

[21]. KenGen, "Geoscientific Study of Eburru-Badlands- Elementaita Geothermal Prospect," 2017.

[22]. P. A. Omenda, "Geothermal Exploration in Kenya," United Nations Univeristy-Geothermal Dev. Co. Short Course V, p. 14, 2010.

[23]. K. Valizadeh Kamran, M. Pirnazar, and V. Farhadi Bansouleh, "Land surface temperature retrieval from Landsat 8 TIRS: comparison between split window algorithm and SEBAL method," Third Int. Conf. Remote Sens. Geoinf. Environ., vol. 9535, p. 953503, 2015.

[24]. Q. Qin, N. Zhang, P. Nan, and L. Chai, "Geothermal area detection using Landsat ETM+ thermal infrared data and its mechanistic analysis-A case study in Tengchong, China," Int. J. Appl. Earth Obs. Geoinf., vol. 13, no. 4, pp. 552–559, 2011.

[25]. J. A. Sobrino, J. C. Jiménez-Munoz, J. El-Kharraz, M. Gómez, M. Romaguera, and G. Sòria, "Single-channel and two-channel methods for land surface temperature retrieval from DAIS data and its application to the Barrax site," Int. J. Remote Sens., vol. 25, no. 1, pp. 215–230, 2004.

[26]. Z. Qin, A. Karnieli, and P. Berliner, "A mono-window algorithm for retrieving land surface temperature from Landsat TM data and its application to the Israel-Egypt border region," Int. J. Remote Sens., vol. 22, no. 18, pp. 3719–3746, 2001.

[27]. M. Eneva, M. Coolbaugh, and J. Combs, "Application of Satellite Thermal Infrared Imagery to Geothermal Exploration in East Central California," GRC Trans., vol. 30, pp. 407–412, 2006.

[28]. S. Ke-Sheng and H. Ming-Yuan, "Application of Remote Sensing Technology in Geothermal Exploration: a Case Study of Taizhou City in Jiangsu Province," Proc. World Geotherm. Congr. 2010, vol. 1100, no. April, pp. 25–29, 2010.

[29]. R. G. Vaughan, J. B. Lowenstern, L. P. Keszthelyi, C. Jaworowski, and H. Heasler, "Mapping Temperature and Radiant Geothermal Heat Flux Anomalies in the Yellowstone Geothermal System Using ASTER Thermal Infrared Data," GRC Trans., vol. 36, no. 2001, pp. 1403–1409, 2012.

[30]. J. Mutua, a Friese, F. Kuehn, T. Lopeyok, M. Mutonga, and N. Ochmann, "High Resolution Airborne Thermal Infrared Remote Sensing Study , Silali Geothermal Prospect , Kenya," Short Course VIII Explor. Geotherm. Resour., pp. 1–10, 2013.

[31]. X. Yu, X. Guo, and Z. Wu, "Land surface temperature retrieval from landsat 8 TIRS-comparison between radiative transfer equation-based method, split window algorithm and single channel method," Remote Sens., vol. 6, no. 10, pp. 9829–9852, 2014.

[32]. P. Omenda, S. Simiyu, and G. Muchemi, "Geothermal Country Update Report for Kenya : 2014," in ARGeo-C5, 2014, no. Figure 1, pp. 29–31.

Cite this article as:

Kathurima C. Eric, "Using Landsat-8 Data in Preliminary Exploration for Geothermal Resources", International Journal of Scientific Research in Science, Engineering and Technology (IJSRSET), Online ISSN: 2394-4099, Print ISSN: 2395-1990, Volume 6 Issue 3, pp. 223-240, May-June 2019. Available at doi: https://doi.org/10.32628/IJSRSET196312

Journal URL: http://ijsrset.com/IJSRSET196312